Centimeter-Level 3D Mobile Online Visible Light Positioning System With Single LED-Lamp

Shuai Ma, Bing Li, GuanJie Zhang, Hang Li, Chen Qiu, Chuang Yu, Shiyin Li, and Chao Shen

***Abstract*—In this paper, we consider a practical indoor 3D mobile online visible light positioning (VLP) system, where the orientation of the UE is arbitrary. Based on the received signal strength (RSS) of multiple photo-detectors (PDs), we formulate the 3D VLP problem as a non-linear least squares (NLS) optimization problem, and then propose a sequential quadratic programming (SQP) positioning algorithm to efficiently calculate UE's location. To obtain more accurate positioning solutions, we further leverage the advantages of deep learning and develop a stochastic gradient descent (SGD) based VLP algorithm, and achieve an average positioning error of 1.77cm, which significantly outperforms existing RSS VLP localization methods. Moreover, we design a 3D mobile online VLP system prototype by using a portable RaspberryPi 4 Model B as the positioning signal processor and data memory, and establish the first publicly available 3D VLP measured dataset including both RSS and orientation. The proposed positioning schemes are implemented and evaluated via the designed prototype system, which can achieve centimeter-level positioning accuracy (below 1 cm in certain condition).**

***Index Terms*—Visible light positioning, received signal strength, arbitrary orientation.**

I. Introduction

The indoor positioning technology has attracted significant attentions due to its key role in numerous location-aware services, including, but not limited to, indoor navigation, asset tracking, human activity recognition, and intelligent logistics system. By utilizing the widely deployed light emitting diode (LED), visible light positioning (VLP) can simultaneously provide high-accuracy localization and illumination services. Compared with other existing indoor positioning technologies, such as wireless fidelity (WiFi) positioning [1], radio frequency identification (RFID) [2], magnetic information [3], bluetooth [4], and ultra-wideband (UWB) [5], VLP exhibits the advantages of high positioning accuracy, license-free spectrum, energy-efficient, low multi-path effects, high security, and no electromagnetic interference, etc. Furthermore, VLP can be widely applied in electromagnetic sensitive areas, where RF radiation is potentially hazardous or even forbidden, e.g., hospitals, nuclear power plants, and mines.

In VLP systems, various techniques can be leveraged for position estimation, such as image sensing [6], [7], received signal strength (RSS) [8], time-of-arrival (TOA) [9] [10], time-difference-of-arrival (TDOA) [11] and angle-of-arrival (AOA) [12]. Specifically, the image sensing positioning method requires complicated image sensor hardware (cameras) as the receiver. AOA, TOA and TDOA based indoor positioning methods require complex signal processing [13], and while RSS is the most commonly-used VLP method due to its easy implementation and low-cost characteristics.

According to the required number of lamps, RSS based VLP technology can be further classified into multi-lamps positioning schemes [14], [15] and single-lamp positioning schemes [16], where the lamp is utilized as the anchor node for positioning. However, the multi-lamps positioning schemes in general require at least three anchors for effective localization, which is hard to implement in many practical VLC applications area. For example, in a long corridor or tunnel, the lamps are deployed along a line with large intervals. In these scenarios, multiple lamps may not be visible to the user equipments (UEs) at the same time. To overcome the practical application limitations, the single-lamp VLP schemes were proposed [8], [12], [14], [16], [17]. Specifically, the triangulation positioning methods were developed for 2D [14] and 3D [8] VLP, respectively. Using AOA and RSS, a 3D indoor positioning system was proposed in [12] with the fixed PD orientation. In [16], a 2D positioning algorithm was presented based on a long short term memory-fully connected network (LSTM-FCN). Fixing the PD orientation, a weighted k-nearest neighbor (KNN) algorithm was applied in [17] for 2D fingerprinting localization. The features and the performance of the above works are summarized in Table I. Note that, the existing VLP works only consider 3D (or 2D) positioning with upward (or fixed) PD orientation. In practice, the PDs' orientation of mobile users may not be fixed and can be arbitrary.

Manuscript received January 25, 2022; revised June 29, 2022 ,December 23, 2022 and May 29, 2023; accepted June 02, 2023. The work of S. Ma was supported by the National Key Research and Development Program of China (No. 2019YFA0706604), the Natural Science Foundation (NSF) of China (Nos. 61976169, 62293483). The work of S. Li was supported by the National Natural Science Foundation of China under Grant 61771474. The work of C. Qiu was supported by the National Natural Science Foundation of China under Grant 62101293, China Postdoctoral Science Foundation under Grant 2021M701806, and the Major Key Project of PCL. The associate editor coordinating the review of this article and approving it for publication was Professor Wei-Shinn Ku. (Corresponding author: Shiyin Li.)

S. Ma is with the Peng Cheng Laboratory, Shenzhen 518055, China, and also with the School of Information and Control Engineering, China University of Mining and Technology, Xuzhou, 221116, China. (e-mail: mash01@pcl.ac.cn).

B. Li, G. Zhang and S. Li are with the School of Information and Control Engineering, China University of Mining and Technology, Xuzhou, 221116, China. (e-mail: { lb_1015, zhangguanjie, lishiyin}@cumt.edu.cn).

H. Li is with the Shenzhen Research Institute of Big Data, Shenzhen 518172, Guangdong, China. (email: hangdavidli@163.com).

C. Qiu is with the Peng Cheng Laboratory, Shenzhen 518000, China (e-mail: qiuch@pcl.ac.cn).

C. Yu is with Cognitive Robotics Lab, Department of Computer Science, University of Manchester, Manchester M13 9PL, United Kingdom (e-mail: chuang.yu@ucl.ac.uk).

C. Shen is with Shenzhen Research Institute of Big Data, Shenzhen, China (e-mail: chaoshen@sribd.cn).

TABLE I: Comparison with existing positioning works.

Work	Method	Areas $(\mathrm{L, W, H})\,\mathrm{m}^3$	Lamp	2D /3D	Accuracy (cm)	Notes	On/Off line	Receiver Orientation θ	SNR (dB)
[8]	Tri.	$(1, 1, 0)$	1	2D	2.15	Exp.	Off	0°	/
[18]	Tri.	$(0.25, 0.25, 0)$	3	2D	1.68	Exp.	Off	0°	/
[7]	Tri.	$(1.8, 1.8, 0)$	1	2D	2.26	Exp.	On	0°	/
[14]	Tri.	$(6, 6, 0)$	6	2D	4-6	Exp.	Off	0°	/
[19]	Tri.	$(1.5, 1.2, 0)$	4	2D	25	Exp.	On	0°	15-60
[20]	Tri.	$(0.6, 0.6, 0)$	4	2D	4/8	Exp.	On	0°	42-56
[21]	Tri.	$(1, 1, 0)$	4	2D	1	Sim.	Off	0°	10
[22]	Tri.	$(5, 5, 0)$	5	2D	3.3	Exp.	On	0°	25
LS	Tri.	$(3, 3, 2.2)$	1	3D	16.8	Exp.	On	0°	8.5
LS	Tri.	$(3, 3, 2.2)$	1	3D	26.36	Exp.	On	Arbitrary	8.5
[23]	DL	$(1.2, 1.2, 2)$	3	3D	11.93	Exp.	Off	0°	/
[24]	DL	$(1, 1.1, 2.5)$	3	3D	3.65	Exp.	Off	0°	/
[17]	DL	$(1.2, 1.2, 0)$	4	2D	1	Exp.	Off	0°	/
[15]	DL	$(5, 5, 0)$	4	2D	2.48	Sim.	Off	0°	/
[16]	DL	$(1, 1.1, 0)$	1	2D	0.92	Exp.	Off	0°	/
[25]	DL	$(0.5, 0.6, 0.8)$	3	3D	3.16	Sim.	Off	0°	/
[26]	DL	$(1, 1, 0)$	3	2D	4.9	Exp.	On	0°	/
[27]	DL	$(8, 8, 0)$	3	2D	3.4	Sim.	Off	0°	29
[28]	DL	$(1, 1, 0)$	4	2D	0.7	Exp.	On	0°	/
SGD	DL	$(3, 3, 2.2)$	1	3D	0.7	Exp.	On	0°	8.5
SGD	DL	$(3, 3, 2.2)$	1	3D	1.77	Exp.	On	Arbitrary	8.5

In this paper, for a 3D VLP system, we develop a least squares (LS) positioning scheme and a stochastic gradient descent (SGD) positioning scheme for arbitrary UE orientation, as well as the vertical up UE orientation (like most existing works did). More specifically, the main contributions of this work are summarized as follows:

- Based on the RSS at the multi-PDs, we first formulate 3D VLP problem with arbitrary UE orientation as a non-linear least square (NLS) optimization problem by exploiting the Lambertian channel model, which is non-convex and difficult to find the optimal solutions. To overcome this difficulty, we propose a sequential quadratic programming (SQP) positioning algorithm to iteratively solve the NLS problem, where the iteration step-sizes are updated according to Wolfe-Powell rule. The proposed SQP scheme can achieve the positioning error of 16.8cm for the vertical up orientation, and 26.36cm for the arbitrary orientation.
- Since the 3D VLP problem is a nonlinear and non-convex problem, the above proposed SQP algorithms may fall into poor local optimal positioning solutions. To further improve the positioning accuracy, we explore the advantages of deep learning to solve the nonlinear and non-convex 3D VLP problem. More specific, we design SGD based VLP schemes for the arbitrary and vertical up PDs orientation, respectively. The SGD based VLP schemes can achieve 0.7cm for the vertical up PDs orientation, and 1.77 cm for the arbitrary PDs orientation, which can significantly outperform existing RSS VLP localization methods (referring to Table I).
- We further design and implement a 3D online single-lamp-multi-PDs positioning system prototype. By using a portable RaspberryPi 4 Model B as the positioning signal processor and data memory, the light intensity of multiple PDs and IMU orientation data are collected simultaneously. Then, we build a RSS and orientation measurements database, which is available at https://pan.baidu.com/s/1GCvxSaKpnqjd1XqSRsfbfg?pwd=nbjy. To the best of our knowledge, this is the first publicly available RSS and orientation measured database of 3D VLP systems, which is free for researchers to perform VLP testing and analysis.

Moreover, we compare the proposed positioning schemes with exiting works in detail from the perspectives of positioning area, number of lamps, positioning dimensions, positioning accuracy, verification methods, processing methods, receiver orientation and SNR, which are listed in Table I. In Table I, “Tri.” means triangulation positioning methods, “DL” means deep learning positioning methods, “Sim.” means simulation results, “Exp.” means experimental results. Specifically, comparing with the existing VLP schemes, the proposed VLP schemes are the first to achieve 3-dimension positioning with arbitrary receiver orientation. Moreover, comparing with the trilateration based VLP schemes, positioning areas of the proposed LS schemes are the largest, and the SNRs of the input signals are the lowest. Comparing with the DL based VLP schemes, the positioning areas of the proposed SGD schemes are the largest, and the SNRs of the input signals of the the proposed SGD schemes are the lowest.

The rest of this paper is organized as follows. In Section II,

This article has been accepted for publication in IEEE Internet of Things Journal. This is the author's version which has not been fully edited and content may change prior to final publication. Citation information: DOI 10.1109/JIOT.2023.3285556

we introduce the 3D VLP system model. In Section III, we develop 3D LS based positioning scheme. In Section IV, we propose the SGD based positioning scheme. In Section V, we present the 3D VLP system prototype design and implementation. Section VI evaluates the performance of the proposed positioning algorithms, and finally the paper is concluded in Section VII.

II. System Model

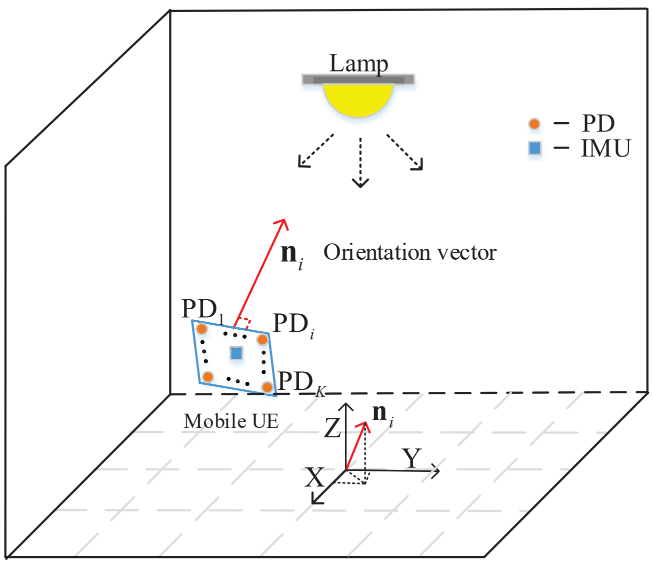

Fig. 1: The 3D VLP system model.

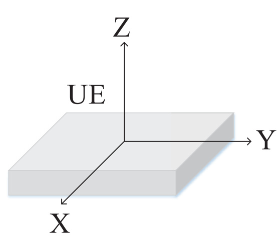

(a) Horizontal.

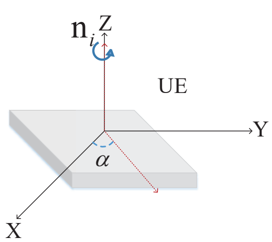

(b) The yaw α.

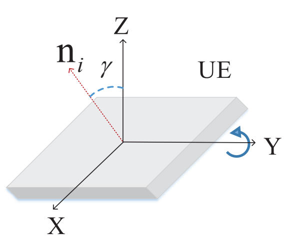

(c) The roll γ.

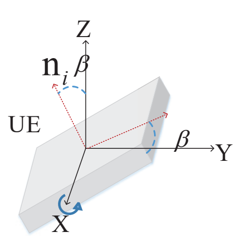

(d) The pitch β.

Fig. 2: User receiver orientation diagram.

Consider a 3D single-lamp-multi-PDs positioning system, as shown in Fig. 1, where the lamp with a single LED in the ceiling serves a mobile user equipment (UE) that has a K PDs and an inertial measurement unit (IMU). Let $\mathbf{u}_{\mathrm{L}} = [\vartheta_1, \vartheta_2, \vartheta_3]^{\mathrm{T}}$ and $\mathbf{u}_i \triangleq [u_{i,1}, u_{i,2}, u_{i,3}]^T$ denote the position of the lamp and the i-th PD, respectively, where $i \in \{1, 2, \cdots, K\}$. Assume that the PDs are placed rigidly on the UE, i.e., all PDs rotate along with the UE. Without loss of generality, assume that the position of the 1st PD represent the position of the UE. As such, the orientation and the rotation angle of the 1st PD are the same as those of UE. Moreover, the orientation of the lamp is vertical downward, i.e. $\mathbf{n}_{\mathrm{L}} = [0, 0, -1]^{\mathrm{T}}$.

Based on Euler's rotation theorem [29], any UE's orientation in $\mathbb{R}^3$ space can be uniquely decomposed by three elemental rotations. Fig. 2 (a) shows the initial vertical up orientation of UE, and three kinds of rotation are given in Fig. 2(b)-(d), respectively. Specifically, α, β, and γ respectively denote rotation angle around the Z-axis, X-axis and Y-axis, which are called yaw, pitch and roll, respectively. The corresponding rotation matrices $\mathbf{R}_\alpha, \mathbf{R}_\beta, \mathbf{R}_\gamma$ are respectively given as

$$\mathbf{R}_\alpha = \begin{bmatrix} \cos\alpha & -\sin\alpha & 0 \\ \sin\alpha & \cos\alpha & 0 \\ 0 & 0 & 1 \end{bmatrix}, \tag{1a}$$

$$\mathbf{R}_\beta = \begin{bmatrix} 1 & 0 & 0 \\ 0 & \cos\beta & -\sin\beta \\ 0 & \sin\beta & \cos\beta \end{bmatrix}, \tag{1b}$$

$$\mathbf{R}_\gamma = \begin{bmatrix} \cos\gamma & 0 & \sin\gamma \\ 0 & 1 & 0 \\ -\sin\gamma & 0 & \cos\gamma \end{bmatrix}. \tag{1c}$$

The concatenated rotation matrix can be written as $\mathbf{R} = \mathbf{R}_\alpha \mathbf{R}_\beta \mathbf{R}_\gamma$, which is explicitly given as

$$\mathbf{R} = \begin{bmatrix} \cos\gamma \sin\alpha \sin\beta + \cos\alpha \sin\gamma \\ \sin\alpha \sin\gamma - \cos\alpha \cos\gamma \sin\beta \\ \cos\beta \cos\gamma \end{bmatrix}. \tag{2}$$

Therefore, the orientation of the i-th PD can be expressed as $\mathbf{n}_i = \mathbf{R}\mathbf{n}_{0,i}$, where $\mathbf{n}_{0,i} \in \mathbb{R}^{3\times 1}$ denote the initial orientation of the i-th PD. Furthermore, after the rotation, the position of the i-th PD is given as

$$\mathbf{u}_i = \mathbf{u}_1 + \mathbf{a}_i, \tag{3}$$

where $\mathbf{a}_i = \mathbf{R}\mathbf{a}_{0,i}$ denotes the position bias of the i-th PD, $\mathbf{u}_1$ is the position of the 1st PD, and $\mathbf{a}_{0,i} \in \mathbb{R}^{3\times 1}$ denotes the position bias relative to the 1st PD in the initial position.

Let $h_i(t)$ denote the VLC channel between BS and the i-th PD at time t, which includes both the line-of-sight (LOS) link and the diffused reflection link. Mathematically, the VLC channel gain $h_i(t)$ is given as [30], [31]

$$h_i(t) = h_{\mathrm{L},i}\delta(t) + h_{\mathrm{d},i}(t - \Delta T_i), \tag{4}$$

where $h_{\mathrm{L},i}$ and $h_{\mathrm{d},i}(t - \Delta T_i)$ denote the gains of the LOS channel and diffused reflection channel, respectively, $\delta(t)$ is the Dirac function, and ΔT_i denotes the time delay of the non-line-of-sight (NLOS) path. Furthermore, according to Lambertian channel model, the LOS channel gain $h_{\mathrm{L},i}$ is given by [32]

$$h_{\mathrm{L},i} = \frac{(m+1)\,A_{\mathrm{PD},i}}{2\pi d_i^2} g_{\mathrm{f}} \cos^m(\phi_i)\cos(\psi_i)\,\mathrm{rect}\left(\frac{\psi_i}{\Psi_c}\right), \tag{5}$$

where $m = -\ln 2/\ln\left(\cos\Phi_{1/2}\right)$ denotes the the Lambertian emission order, $\Phi_{1/2}$ is the semi-angle at half power. $A_{\mathrm{PD},i}$ represents the receiving area of the i-th PD, g_{f} is the gain of the optical concentrator, d_i denotes the distance between BS and the i-th PD, ϕ_i represents the angle between the emitted light and the normal vector of the LED. ψ_i is the angle between the emitted light and the normal vector of the i-th PD, and Ψ_c stands for field of view (FOV) of PD. Moreover, $\mathrm{rect}\left(\psi_i/\Psi_c\right)$ is given by

$$\mathrm{rect}\left(\frac{\psi_i}{\Psi_c}\right) = \begin{cases} 1, & 0 \le \psi_i \le \Psi_c, \\ 0, & \text{otherwise}, \end{cases} \tag{6}$$

where $i \in \mathcal{K}$.

By taking the position $\mathbf{u}_i = \mathbf{u}_1 + \mathbf{a}_i$ and the angle into consideration, we have

$$h_{\mathrm{L},i} = \frac{\gamma_i(\vartheta_3 - \theta_{3,i})^m(\mathbf{u}_{\mathrm{L}} - \mathbf{u}_1 - \mathbf{a}_i)^{\mathrm{T}}\mathbf{n}_i}{\|\mathbf{u}_{\mathrm{L}} - \mathbf{u}_1 - \mathbf{a}_i\|^{m+3}\|\mathbf{n}_i\|}, \tag{7}$$

where $\gamma_i \triangleq \frac{(m+1)A_{\mathrm{PD},i}g_{\mathrm{f}}}{2\pi}$, and $d_i = \|\mathbf{u}_{\mathrm{L}} - (\mathbf{u}_1 + \mathbf{a}_i)\|$.

Furthermore, let $H_i(f)$ denote the frequency domain channel gain of the i-th PD $h_i(t)$, which is given by

$$H_i(f) = h_{\mathrm{L},i} + c_{d,i}, \tag{8}$$

where $c_{\mathrm{d},i}$ is the power efficiency for the diffuse signal. In addition, $c_{\mathrm{d},i}$ is given by

$$c_{\mathrm{d},i} = \frac{\rho A_{\mathrm{PD},i} e^{j2\pi f \Delta T_i}}{(1-\rho)A_{\mathrm{room}}\left(1 + j\frac{f}{f_0}\right)}, \tag{9}$$

where A_{room} represents the surface area of room,f_0 stands for the cutoff frequency and ρ is the average reflectivity of the room.

In the VLP system, the transmitted signal of the LED $x(t)$ is given as

$$x(t) = \sqrt{P}s(t) + I_{\mathrm{DC}}, \tag{10}$$

where P denotes the power gain of the power amplifier of the LED driver, $s(t)$ denotes the united power signal, i.e., $\mathrm{E}\left\{s^2(t)\right\} = 1$, and I_{DC} stands for the DC bias. Thus, the received signal of the i-th PD $y_i(t)$ is given as

$$y_i(t) = h_i(t) * x(t) + z_i(t), \tag{11}$$

where $z_i(t) \sim \mathcal{N}(0, \sigma_i{}^2)$ denotes the additive white Gaussian noise (AWGN). Therefore, the received power of the i-PD is given as

$$P_{y,i} = \frac{1}{T}\int_0^T (h_{\mathrm{L,i}} + c_{d,i})^2 x(t)^2 dt + \sigma_i^2 \tag{12a}$$

$$= \left(h_{\mathrm{L},i}^2 + c_{d,i}^2 + 2h_{\mathrm{L,i}}c_{d,i}\right)P_s + \sigma_i^2, \tag{12b}$$

where T represents the symbol period of the transmitted signal.

III. Non-linear Least Squares Positioning Schemes

In this section, we investigate the NLS positioning scheme by taking the arbitrary PDs orientation into consideration, where the orientation information is obtained from the IMU at the UE.

Since the received power of the PD is a function of UE's location, the location can be jointly calculated based on the the received power of multi-PDs. Specifically, the received power of PDs $\{P_{y,i}\}_{i=1}^K$ in (12b) can be reformulated as

$$h_{\mathrm{L},i} = \sqrt{\frac{P_{y,i} - \sigma_i^2}{P_s}} - c_{\mathrm{d},i}. \tag{13}$$

Combining (7) and (13), we have

$$\sqrt{\frac{P_{y,i} - \sigma_i^2}{P_s}} - c_{\mathrm{d},i} = \frac{\gamma_i\left(\vartheta_3 - \theta_{3,i}\right)^m(\mathbf{u}_{\mathrm{L}} - \mathbf{u}_1 - \mathbf{a}_i)^{\mathrm{T}}\mathbf{n}_i}{\|\mathbf{u}_{\mathrm{L}} - \mathbf{u}_1 - \mathbf{a}_i\|^{m+3}\|\mathbf{n}_i\|}. \tag{14}$$

Since there are K PDs at UE, the UE's position $\mathbf{u}_1$ can be obtained by solving following equations

$$\begin{cases} \sqrt{\frac{P_{y,1}-\sigma_1^2}{P_s}} - c_{\mathrm{d},1} = \frac{\gamma_1\left(\vartheta_3 - \theta_{3,1}\right)^m(\mathbf{u}_{\mathrm{L}} - \mathbf{u}_1)^{\mathrm{T}}\mathbf{n}_1}{\|\mathbf{u}_{\mathrm{L}} - \mathbf{u}_1\|^{m+3}\|\mathbf{n}_1\|}, \\ \qquad\vdots \\ \sqrt{\frac{P_{y,K}-\sigma_K^2}{P_s}} - c_{\mathrm{d},K} = \frac{\gamma_K\left(\vartheta_3 - \theta_{3,k}\right)^m(\mathbf{u}_{\mathrm{L}} - \mathbf{u}_1 - \mathbf{a}_K)^{\mathrm{T}}\mathbf{n}_K}{\|\mathbf{u}_{\mathrm{L}} - \mathbf{u}_1 - \mathbf{a}_K\|^{m+3}\|\mathbf{n}_K\|}. \end{cases} \tag{15}$$

Note that, there are $(K+3)$ variables in (15), i.e., $\{c_{d,i}\}_{i=1}^K$ and $\mathbf{u}_1$, which is an under-determined equation with infinite solutions. Since the values of NLOS terms $\{c_{d,i}\}_{i=1}^K$ are significantly lower than that of LOS term $h_{\mathrm{L,i}}$, we approximate the values of $\{c_{d,i}\}_{i=1}^K$ to be the same, i.e., $c_{d,i} = c_d, \forall i$. Thus, the equations (15) can be re-expressed as

$$\begin{cases} \sqrt{\frac{P_{y,1}-\sigma_1^2}{P_s}} - c_{\mathrm{d}} = \frac{\gamma_1\left(\vartheta_3 - \theta_{3,1}\right)^m(\mathbf{u}_{\mathrm{L}} - \mathbf{u}_1)^{\mathrm{T}}\mathbf{n}_1}{\|\mathbf{u}_{\mathrm{L}} - \mathbf{u}_1\|^{m+3}\|\mathbf{n}_1\|}, \\ \qquad\vdots \\ \sqrt{\frac{P_{y,K}-\sigma_K^2}{P_s}} - c_{\mathrm{d}} = \frac{\gamma_K\left(\vartheta_3 - \theta_{3,k}\right)^m(\mathbf{u}_{\mathrm{L}} - \mathbf{u}_1 - \mathbf{a}_K)^{\mathrm{T}}\mathbf{n}_K}{\|\mathbf{u}_{\mathrm{L}} - \mathbf{u}_1 - \mathbf{a}_K\|^{m+3}\|\mathbf{n}_K\|}. \end{cases} \tag{16}$$

For convenience, we introduce the following variables

$$r_i(\mathbf{u}_1) \triangleq \frac{\sqrt{P_{y,i} - \sigma_i^2}}{P_s} - c_d - \frac{\gamma_i(\vartheta_3 - \theta_{3,i})^m(\mathbf{u}_{\mathrm{L}} - \mathbf{u}_1 - \mathbf{a}_i)^{\mathrm{T}}\mathbf{n}_i}{\|\mathbf{u}_{\mathrm{L}} - \mathbf{u}_1 - \mathbf{a}_i\|^{m+3}\|\mathbf{n}_i\|}, \tag{17}$$

$$\mathbf{r}(\mathbf{u}_1) \triangleq [r_1(\mathbf{u}_1), r_2(\mathbf{u}_1), \ldots, r_K(\mathbf{u}_1)]^{\mathrm{T}}, \tag{18}$$

$$f(\mathbf{u}_1) \triangleq \frac{1}{2}\|\mathbf{r}(\mathbf{u}_1)\|^2. \tag{19}$$

Then, the equations (16) can be equivalently formulated as a NLS optimization problem given by

$$\min_{\mathbf{u}_1} \quad f(\mathbf{u}_1) = \frac{1}{2}\|\mathbf{r}(\mathbf{u}_1)\|^2, \tag{20}$$

which is non-convex and difficult to find the optimal solutions. To overcome this difficulty, we exploit the SQP algorithm [33] to iteratively solve the NLS problem. Specifically, the $(i+1)$th iteration point $\mathbf{u}_1^{[i+1]}$ is updated as

$$\mathbf{u}_1^{[i+1]} = \mathbf{u}_1^{[i]} + \mathbf{d}^{[i]}, \tag{21}$$

This article has been accepted for publication in IEEE Internet of Things Journal. This is the author's version which has not been fully edited and content may change prior to final publication. Citation information: DOI 10.1109/JIOT.2023.3285556

where $\mathbf{d}^{[i]} = \alpha_i \eta^{[i]}$ represents the descending direction vector corresponding to the i-th iteration, α_i denotes the stepsize, and $\eta^{[i]} \in \mathbb{R}^{3\times 1}$ denotes the descending direction. The optimal descending direction $\eta^{[i]}$ satisfies the following equation

$$\mathrm{H}\left(\mathbf{u}_1^{[i]}\right)\eta^{[i]} = -\nabla f\left(\mathbf{u}_1^{[i]}\right), \tag{22}$$

where $\nabla f\left(\mathbf{u}_1^{[i]}\right)$ and $\mathrm{H}\left(\mathbf{u}_1^{[i]}\right)$ denote the gradient and the Hessian matrix of $f\left(\mathbf{u}_1^{[i]}\right)$, respectively. Furthermore, $\mathrm{H}\left(\mathbf{u}_1^{[i]}\right)$ is given as

$$\mathrm{H}\left(\mathbf{u}_1^{[i]}\right) = \begin{bmatrix} \frac{\partial^2 f\left(\mathbf{u}_1^{[i]}\right)}{\partial \mathrm{u}_1^2} & \frac{\partial^2 f\left(\mathbf{u}_1^{[i]}\right)}{\partial u_1 \partial u_2} & \cdots & \frac{\partial^2 f\left(\mathbf{u}_1^{[i]}\right)}{\partial u_1 \partial u_k} \\ \frac{\partial^2 f\left(\mathbf{u}_1^{[i]}\right)}{\partial u_2 \partial u_1} & \frac{\partial^2 f\left(\mathbf{u}_1^{[i]}\right)}{\partial u_2^2} & \cdots & \frac{\partial^2 f\left(\mathbf{u}_1^{[i]}\right)}{\partial u_2 \partial u_k} \\ \vdots & \vdots & \ddots & \vdots \\ \frac{\partial^2 f\left(\mathbf{u}_1^{[i]}\right)}{\partial u_k \partial u_1} & \frac{\partial^2 f\left(\mathbf{u}_1^{[i]}\right)}{\partial u_k \partial u_2} & \cdots & \frac{\partial^2 f\left(\mathbf{u}_1^{[i]}\right)}{\partial u_k^2} \end{bmatrix}. \tag{23}$$

To choose a proper step-size with a sufficient decrease, the step-size α_i is calculated according to the Wolfe-Powell rule, i.e.,

$$f\left(\mathbf{u}_1^{[i]} + \alpha_i \eta^{[i]}\right) \le f\left(\mathbf{u}_1^{[i]}\right) + \rho \alpha_i \nabla f\left(\mathbf{u}_1^{[i]}\right)^{\mathrm{T}} \eta^{[i]}, \tag{24a}$$

$$\nabla f\left(\mathbf{u}_1^{[i]} + \alpha_i \eta^{[i]}\right)^{\mathrm{T}} \eta^{[i]} \ge \xi \nabla f\left(\mathbf{u}_1^{[i]}\right)^{\mathrm{T}} \eta^{[i]}, \xi \in (\rho, 1), \tag{24b}$$

where $\rho \in (0, 0.5)$ and $\xi \in (\rho, 1)$ are given parameters. In summary, the proposed SQP positioning algorithm is presented in **Algorithm 1**.

Algorithm 1 SQP Positioning Algorithm

Initialize $\mathbf{u}_1^{[0]}$, step-size $\alpha_0 = 1$ and the convergence tolerance $0 < \mu < 1$;
repeat
    Calculate $\mathbf{r}(\mathbf{u}_1^{[i]})$ and the Hessian matrix $\mathrm{H}\left(\mathbf{u}_1^{[i]}\right)$;
    Update the descending direction $\eta^{[i]}$ in (22);
    Calculate the step-size α_i by Wolfe-Powell rule in (24);
    Update $\mathbf{u}_1^{[i+1]} = \mathbf{u}_1^{[i]} + \alpha_i \eta^{[i]}$;
    $i \leftarrow i + 1$;
until $\frac{\left\|\mathbf{u}_1^{[i-1]} - \mathbf{u}_1^{[i]}\right\|}{\left\|\mathbf{u}_1^{[i]}\right\|} \le \mu$;
Output the location solution $\mathbf{u}_1^{[i+1]}$.

For some practical VLP applications, the orientation of PDs may keep vertical up, such as robot cars, cargo tags, which is a special case of arbitrary PDs orientation. In this special case, $\mathbf{n}_i = \mathbf{e}_3 = [0, 0, 1]^T$, $\forall\, i = 1, ..., K$, and the equations (15) can be further simplified as

$$h_{\mathrm{L},i} = \frac{\gamma_i (\vartheta_3 - \theta_{3,i})^m (\mathbf{u}_{\mathrm{L}} - \mathbf{u}_1 - \mathbf{a}_i)^{\mathrm{T}} \mathbf{e}_3}{\|\mathbf{u}_{\mathrm{L}} - \mathbf{u}_1 - \mathbf{a}_i\|^{m+3}}. \tag{25}$$

Furthermore, the objective function of the NLS problem (20) can be rewrote as

$$r_i(\mathbf{u}_1) = \frac{\sqrt{P_{y,i} - \sigma_i^2}}{P_s} - c_d - \frac{\gamma_i (\vartheta_3 - \theta_{3,i})^m (\mathbf{u}_{\mathrm{L}} - \mathbf{u}_1 - \mathbf{a}_i)^{\mathrm{T}} \mathbf{e}_3}{\|\mathbf{u}_{\mathrm{L}} - \mathbf{u}_1 - \mathbf{a}_i\|^{m+3}}. \tag{26}$$

Therefore, the proposed SQP positioning Algorithm 1 can also be applied. The performance of Algorithm 1 will be further evaluated in Section VI.

IV. Deep Learning Positioning Schemes

According to (14), the received power $\{P_{y,i}\}_{i=1}^K$ are nonlinear and non-convex functions of the localization $\mathbf{u}_1$. Therefore, there are many local optimal localization solutions for the 3D VLP problem (16). The proposed SQP algorithm may fall into a local optimal solution during the iterative process, which may lead to high positioning errors. Given the above issues, we turn to apply the data-driven method. Particularly, deep learning has flexible and powerful processing capabilities for complex nonlinear and non-convex optimization problem. Here, we propose a SGD based deep learning positioning network to solve the 3D VLP problem.

Specifically, as shown in Fig. 3, the proposed 3D-VLP SGD network includes K_{v} layers, i.e., $\{\mathbf{v}_i\}_{i=1}^{K_{\mathrm{v}}}$, one input layer $\mathbf{v}_0 \in \mathbb{R}^{K+3}$, K_{v} hidden layers $\left\{\mathbf{v}_i \in \mathbb{R}^{L_i}\right\}_{i=1}^{K_{\mathrm{v}}-2}$, and one output layer $\mathbf{v}_{K_{\mathrm{v}}} \in \mathbb{R}^3$. Moreover, let $\mathbf{W}_i = \left[\mathbf{w}_1^{[i]}, ..., \mathbf{w}_{L_i}^{[i]}\right] \in \mathbb{R}^{L_{i+1} \times L_i}$ denote the weight matrix between the ith layer and the $(i+1)$th layer, where $\mathbf{w}_k^{[i]} = \left[w_{k,1}^{[i]}, ..., w_{k,L_{i+1}}^{[i]}\right]^T \in \mathbb{R}^{L_{i+1}}$ denote the weight vector between the ith layer and the nodes of the $(i+1)$th layer for the kth node.

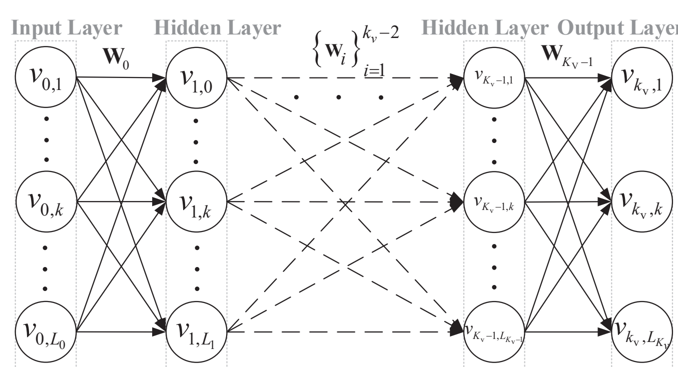

Fig. 3: The proposed SGD positioning network.

The SGD positioning network is trained by multiple small-batch samples. Assume there are N_{b} sampled data vectors $\{\mathbf{b}_1, \cdots, \mathbf{b}_{N_{\mathrm{b}}}\}$ for each batch, where $\mathbf{b}_i = \left[P_{y,1}, ..., P_{y,K}, \mathbf{n}_1^T\right]^T$ denote the ith sample vector of the received power of K PDs and the orientation of the first PD. Moreover, let $\mathbf{u}_1^{(i)}$ denote the corresponding position of the ith sample vector $\mathbf{b}_i$. For the SGD based 3D-VLP network, we first assign the sampled data vectors to the input layer node in sequence, i.e., $\mathbf{v}_0 = \mathbf{b}_i$, where $i = 1, ..., N_{\mathrm{b}}$. Then, the values of the nodes in the ith layer is updated using rectified linear unit (ReLU) activate function, which is given as

$$\mathbf{v}_k = \max\left(\mathbf{0}, \mathbf{W_{k-1}v_{k-1}}\right), \ k = 1, ..., N_{\mathrm{b}}, \tag{27}$$

where $\max(\mathbf{x}, \mathbf{y}) = \{\max(x_i, y_i)\}$ denote the activation function.

Then, the output layer predicts the 3D position vector of the first PD, i.e., $\mathbf{v}_{K_{\mathrm{v}}} \triangleq [\widehat{u}_1, \widehat{u}_2, \widehat{u}_3]$. For the ith sample vector $\mathbf{b}_i$, let $L^{(i)}$ denote the loss function between the predicted position vector $\mathbf{v}_{k_{\mathrm{v}}}$ and the exact position vector (label) $\mathbf{u}_1^{(i)}$, i.e.,

$$L^{(i)}\left(\mathbf{v}_{K_{\mathrm{v}}}, \mathbf{u}_1^{(i)}, \{\mathbf{W}_k\}_{k=0}^{K_{\mathrm{v}}-1}\right) = \left\|\mathbf{v}_{K_{\mathrm{v}}} - \mathbf{u}_1^{(i)}\right\|_2. \tag{28}$$

Therefore, for each batch, the mean loss of the N_{b} sampled vectors is a function of the weight matrix, i.e.,

$$J\left(\{\mathbf{W}_k\}_{k=0}^{K_{\mathrm{v}}-1}\right) = \frac{1}{N_b}\sum_{i=1}^{N_b} L^{(i)}\left(\mathbf{v}_{K_{\mathrm{h}}}, \mathbf{u}_1^{(i)}, \{\mathbf{W}_k\}_{k=0}^{K_{\mathrm{v}}-1}\right). \tag{29}$$

Then, based on the back propagation, the weight matrix $\mathbf{W}$ is updated by

$$\mathbf{W}_l \leftarrow \mathbf{W}_l - \alpha \frac{\partial J\left(\{\mathbf{W}_k\}_{k=0}^{K_{\mathrm{v}}-1}\right)}{\partial \mathbf{W}_l}, l = 0, ..., K_{\mathrm{v}} - 1, \tag{30}$$

where α denotes the step size. In summary, the proposed SGD positioning algorithm is listed in Algorithm 2.

Algorithm 2 SGD Positioning Algorithm

Input: Set the learning rate α, the stop condition parameter $\delta = 1.0 \times 10^{-10}$, number of sample batches N_{b}, and $i = 0$;
while $J\left(\{\mathbf{W}_k\}_{k=0}^{K_{\mathrm{v}}-1}\right) \geq \delta$ **do**
  while $i \leq N_b$ **do**
    Select a batch of samples from the dataset and calculate the value of $L^{(i)}\left(\mathbf{v}_{K_{\mathrm{v}}}, \mathbf{u}_1^{(i)}, \{\mathbf{W}_k\}_{k=0}^{K_{\mathrm{v}}-1}\right)$;
    $i = i + 1$;
  end while
  Calculate $J(\{\mathbf{W}_k\}_{k=0}^{K_{\mathrm{v}}-1})$ in (29);
  Update $\{\mathbf{W}_l\}_{l=0}^{K_{\mathrm{v}}-1}$ according to (30);
end while
Output: $\mathbf{v}_{K_{\mathrm{v}}}$.

When the orientation of PDs is vertical up, the proposed SGD network can be simplified to a lightweight SGD network without IMU input, which requires less numbers of layers and less calculation time. Specifically, a small batch of SGD network is designed for processing, and each batch $\{\mathbf{b}_1, \cdots, \mathbf{b}_{N_{\mathrm{b}}}\}$ includes N_{b} sampled data vectors, where $\mathbf{b}_i = [P_{y,1}, ..., P_{y,K}]^T$ denotes the received power of the ith sample vector of K PDs. Compared with the previous arbitrary case, the inputs of the network is reduced to received power of K PDs, i.e., $\{P_{y,i}\}_{i=1}^K$, and the number of hidden layers is also significantly reduced. In this way, based on the K PDs input data vectors, we may obtain the position of the UE based the simplified Algorithm 2, whose details are omitted for brevity.

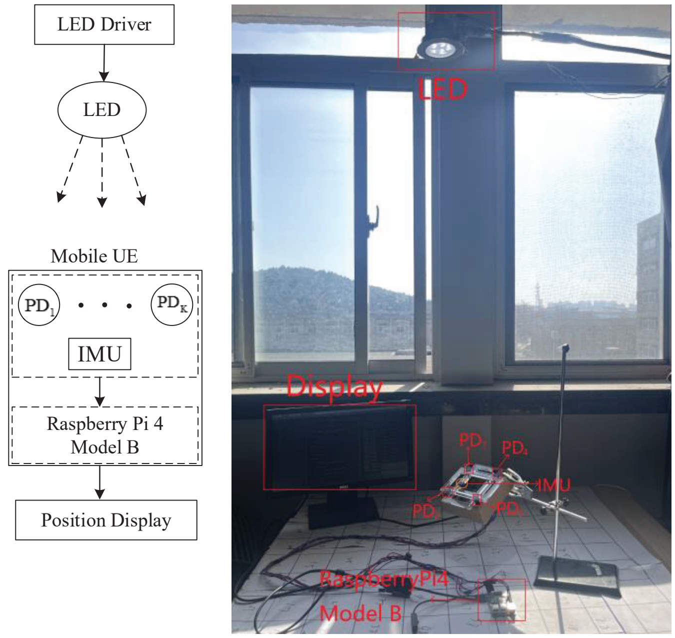

Fig. 4: The proposed 3D VLP prototype.

V. 3D VLP Prototype Design And Implementation

In this section, we introduce the hardware platform design of 3D online VLP system, which can be used to implement the proposed positioning schemes. In the 3D VLP system prototype, the transmitter includes a commercial single LED luminaire and the LED drive control circuit that can adjust the brightness of the light. Note that, for the illumination consideration, multiple LEDs can be integrated in the luminaire as a single anchor node for positioning.

TABLE II: Hardware parameters of 3D online VLP system prototype.

System modules	
Processor	RaspberryPi4 model B
Positioning range(L $\times$ W $\times$ H)	$(300 \times 300 \times 220)cm^3$
LED	5W-LED
TX Driver	9018 Triode
RX Photodiode	TS2516
RX Angle sensor	MPU6050
TX characteristic	
Light Power LED	$(4-7)$W
LEDFoV	120°
Illuminance range	> 1Lux
RX characteristic	
Lambert Coefficient	$m = 1$
photodiode FoV	90°
Ψ_c	90°
Photodiode gain A_{PD}	1
Photodiode receiving area	$1cm^2$

At the VLP receiver side, there are four PDs ($K = 4$) to convert optical signals into electrical signals, and an IMU to measure the real-time orientation of the receiver. The receiver is connected to a portable RaspberryPi 4 Model B processor for data collection and online positioning algorithms processing, and one display is to present the real-time positioning results.

In practice, the received signals may be influenced by the background light and interference. Thus, we further introduce a background noise filtering algorithm, which can automatically detect and eliminate the background light to reduce the impact of background noise. The background noise filtering algorithm (BNF) can significantly improve the robustness of the proposed VLP schemes. The system structure and the prototype are shown in Fig. 4. Our proposed 3D online VLP system prototype can achieve high accuracy positioning in a bright daylight environment.

Training set collection: First, the light intensity data collected by PD and the angle data measured by IMU are synchronized through the our designed software program. Then, in a 3D space of $(300 \times 300 \times 220)\,\mathrm{cm}^3$, each interval of 20cm in the horizontal and vertical directions is a data sampling position point, with a total of 2250 data sampling position point. Each point collects 20 different angles and corresponding light intensities, and there are 45000 sampled training data.

Based on the received light intensity and orientation information, the online positioning schemes are implemented in Python language and executed on the RaspberryPi 4 Model B processor. The detailed parameters of the prototype are provided in Table II. Note that, the data sampling, data training, data preprocessing and the proposed online positioning schemes are all implemented in the proposed positioning prototype system, and the evaluation will be presented in the next section.

VI. Experimental Verification And Theoretical Results

In this section, we evaluate the proposed 3D online VLP schemes via our VLP prototype system. As shown in Fig. 4, our prototype is tested in the laboratory near the window with in the $(1.5 \times 1.5 \times 1.5)\,m^2$ test area. The maximum vertical distance from the LED to PDs is $2m$.

A. LS Positioning Schemes

To verify the accuracy of lambert model, we first test the iso-illuminance spherical surface of the LED. Fig. 5 shows the two-dimensional equal illumination fitting curve of LED with 2700lux. It can be seen from Fig. 5 that the test points with the same illuminance can be approximately fitted into a circle, which verifies the accuracy of the LED spherical lambert radiation model.

Let LS-VU denote the LS scheme with vertical up UE orientation, and LS-AO denote the LS scheme with arbitrary UE orientation. Fig. 6 compares the positioning errors CDF of LS-VU and LS-AO schemes. One can observe that the positioning error of LS-VU scheme is less than that of LS-AO scheme. We conclude that the vertical up orientation can contribute to the positioning accuracy. More specifically, the average positioning errors of LS-VU and LS-AO schemes are 16.8cm and 26.3cm, respectively.

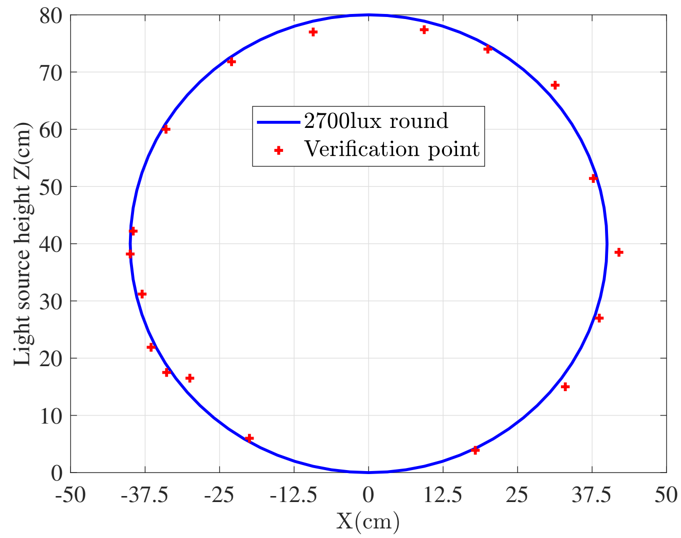

Fig. 5: Two-dimensional iso-illuminance fitting curve of LED with 2700lux.

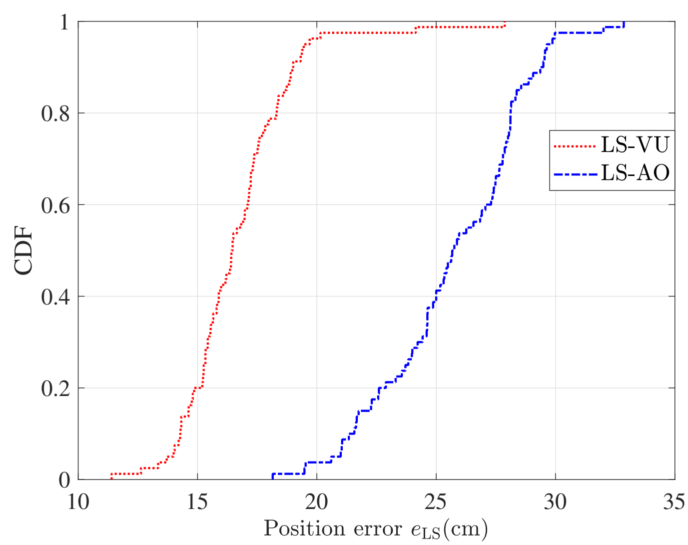

Fig. 6: Positioning errors CDF of the LS VLP schemes.

B. SGD Positioning Schemes

In this section, SGD-AO denotes the SGD scheme with arbitrary UE orientation. Since the performance of deep learning does not increase monotonically with the number of network layers, we first determine the optimal number of layers of the SGD-AO VLP network.

Fig. 7 (a) shows the positioning errors versus the number of layers of the SGD-AO network. It can be seen that the positioning error firstly decreases and then increases as the number of network layers gets large. We may observe that the optimal number of network layers corresponding to the lowest positioning error is 14. Fig. 7 (b) shows the positioning errors versus the number of layers of the SGD-VU (SGD with vertical up UE orientation) network. It can be seen that the positioning errors firstly decreases and then maintains a short fluctuation with the increase of network layers, and has the best positioning accuracy when the number of network layers

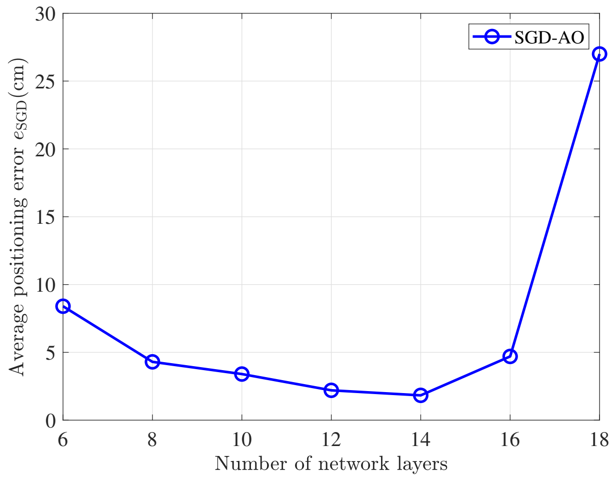

(a)

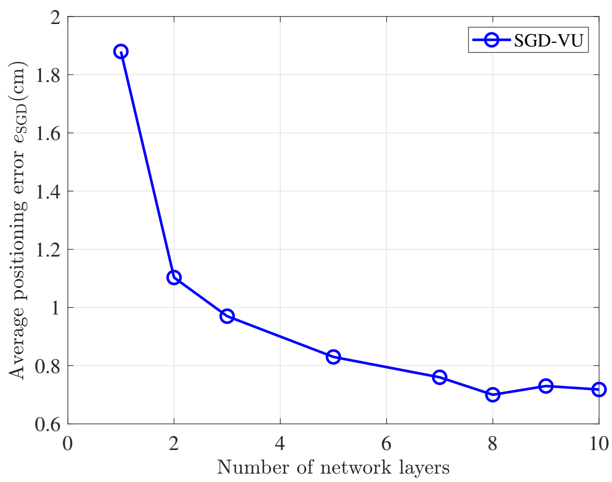

(b)

Fig. 7: (a) Positioning errors versus the number of layers of the SGD-AO network; (b) Positioning errors versus the number of layers of the SGD-VU network.

is 8.

Fig. 8 (a) and (b) depict the positioning errors of SGD-VU network and SGD-AO network versus the number of iterations. It can be seen that the positioning error first declines rapidly, and then tends to be constant as the number of iterations increases. After 600 iterations, the network positioning error converges.

Fig. 9 compares positioning errors CDF of SGD-VU and SGD-AO schemes. It can be seen that the positioning error of SGD-VU network is less than that of SGD-AO network. The average positioning errors of LS-VU and LS-AO schemes are 0.7 cm and 1.77 cm, respectively. Compared with Fig. 6, the average positioning errors of SGD-VU and SGD-AO are significantly lower than those of LS-VU and LS-AO schemes.

Fig. 10 compares positioning errors of SGD-AO and LS-AO schemes which includes 50 random test points. It is observed that, both the mean and variance of the positioning errors of SGD-AO are significantly lower than those of LS-AO schemes.

Fig. 11 illustrates the 3D positioning results of SGD-AO

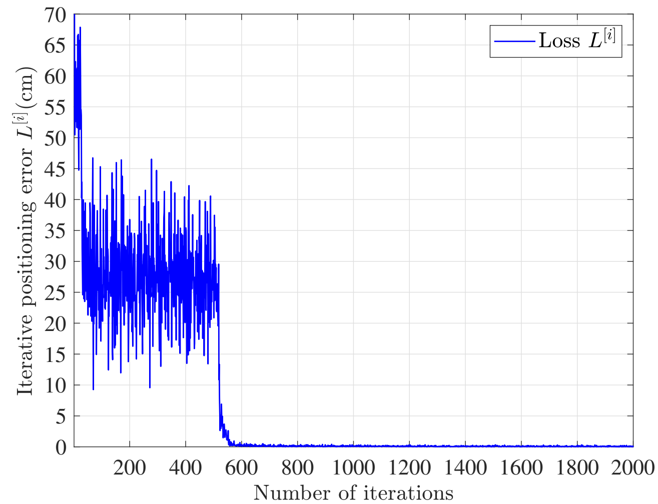

(a)

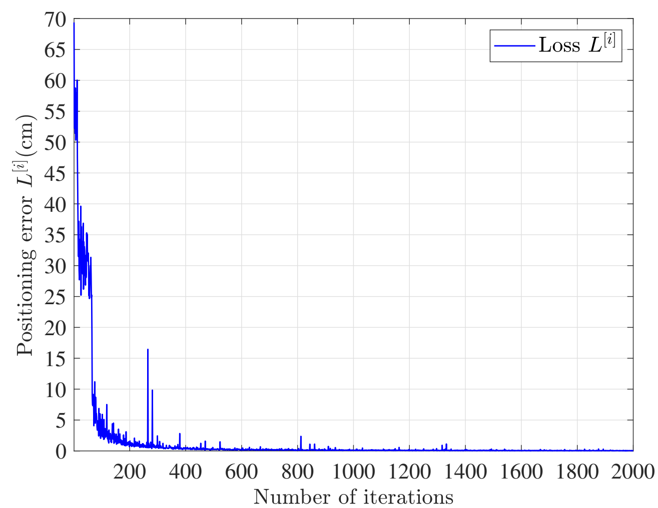

(b)

Fig. 8: (a) Positioning error of SGD-VU network versus number of iterations; (b) Positioning error of SGD-AO network versus number of iterations.

scheme. In Fig. 11, the red dots denote the exact location coordinates and the blue dots denote corresponding positioning results, which verifies the positioning accuracy of the SGD-AO VLP scheme.

Table III compares the computational time, positioning error, number of layers, input dimension, number of nodes and required training data set size of LS-VU, LS-AO, SGD-VU and SGD-AO 3D VLP schemes. From Table III, we can find that the positioning time consuming of LS-VU, LS-AO, SGD-VU and SGD-AO 3D VLP schemes are respectively 680ms, 1200ms, 0.32ms and 0.45ms, where the positioning time consumption of SGD-VU 3D VLP scheme is the shortest. The positioning time of SGD-VU and SGD-AO VLP schemes are significantly lower than those of LS-VU and LS-AO VLP schemes. The reason is that LS-VU and LS-AO VLP schemes employ the SQP Algorithm to iteratively solve the positioning result, while SGD-VU and SGD-AO VLP schemes calculate

TABLE III: Performance comparison among the proposed schemes.

Schemes	Computational time	Positioning error	Number of layers	Input Dimension	Number of nodes	Dataset size
LS-VU	680ms	16.8cm	–	4	–	–
LS-AO	1200ms	26.36cm	–	7	–	–
SGD-VU	0.32ms	0.7cm	8	4	148	500
SGD-AO	0.45ms	1.77cm	14	7	395	2000

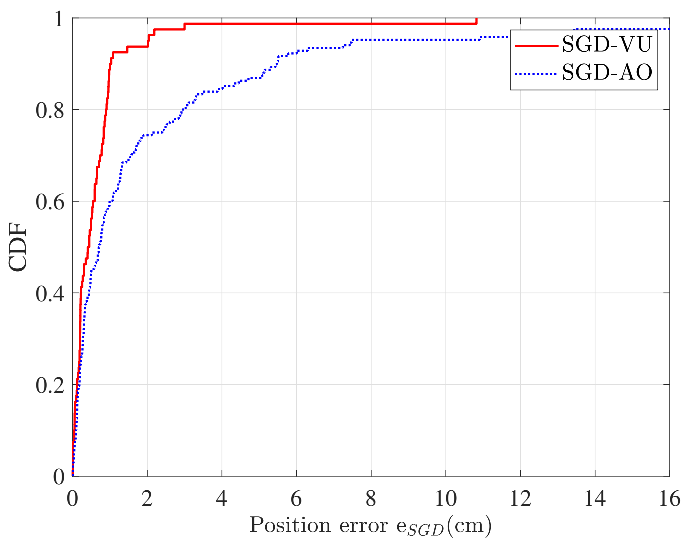

Fig. 9: Positioning errors CDF of SGD-VU and SGD-AO schemes.

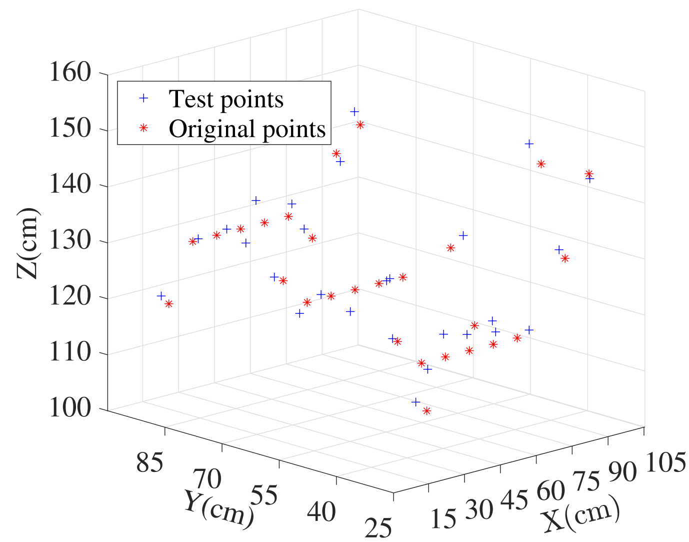

Fig. 11: Illustration of 3D positioning performance of SGD-AO Scheme

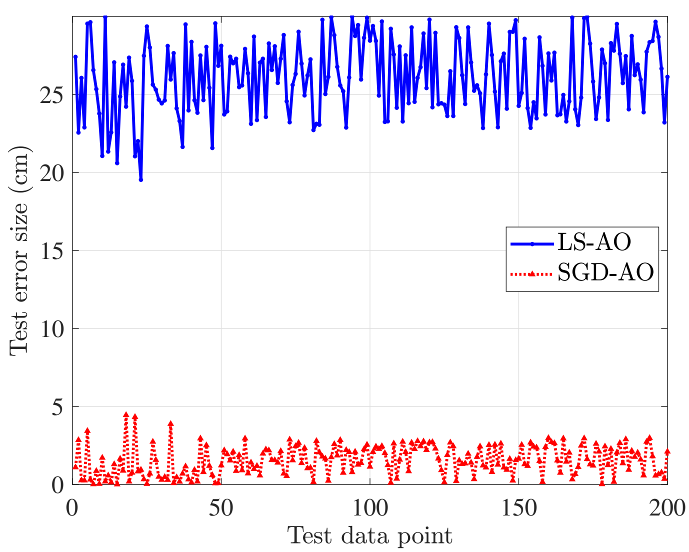

Fig. 10: Positioning performance comparison between LS-AO and SGD-AO schemes.

the position through the pre-trained networks. Table III also shows that the average positioning errors of the four schemes. The average positioning errors of SGD-VU and SGD-AO VLP schemes are significantly lower than those of LS-VU and LS-AO VLP schemes, which is consistent with our above intuition that the SQP algorithm may fall into some local optimum results. Comparing with the SQP algorithm, deep learning based SGD-VU and SGD-AO 3D VLP schemes algorithms can handle complex nonlinear and non-convex optimization problems.

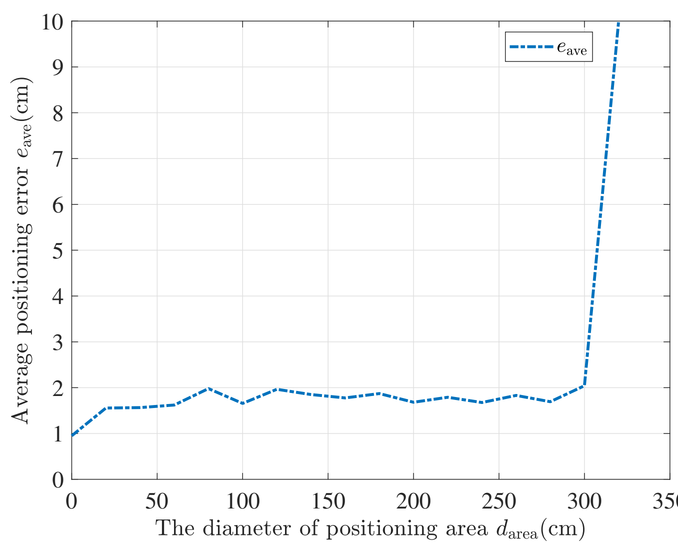

Fig. 12: Positioning error $e_{\rm ave}$ of the proposed SGD-AO network versus positioning area diameter $d_{\rm area}$

Fig. 12 shows the positioning error $e_{\rm ave}$ of the proposed SGD-AO network versus positioning area diameter $d_{\rm area}$. It can be seen that the positioning error is less than 2 cm for

$d_{\text{area}} \leq 3$ m. However, for $d_{\text{area}} > 3$ m, the positioning error increases rapidly. The reason is that it exceeds the effective coverage of the single LED VLP system, and some PDs cannot receive light.

In the proposed VLP hardware platform, the range of the IMU angle error e_{IMU} is $e_{\text{IMU}} \in [-0.1°, 0.1°]$. To illustrate the effect of IMU angle error e_{IMU} on the proposed VLP schemes, we test the CDFs of the positioning accuracy with different e_{IMU}, as shown in Fig. 13.

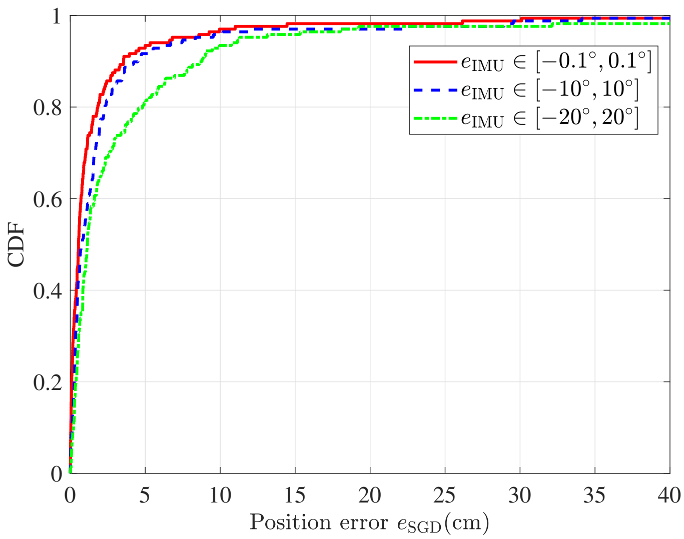

Fig. 13: Positioning accuracy CDF of different IMU angle error e_{IMU}.

Fig. 13 shows positioning accuracy CDF of different IMU angle error e_{IMU}. It can be seen that the positioning accuracy CDFs of $e_{\text{IMU}} \in [-0.1°, 0.1°]$ and $e_{\text{IMU}} \in [-10°, 10°]$ are close, which shows that the proposed VLP schemes are robust to IMU angle errors, especially for error $e_{\text{IMU}} \in [-10°, 10°]$. Moreover, for the large IMU angle error $e_{\text{IMU}} \in [-20°, 20°]$, the positioning performance degrades.

In addition, in order to illustrate the effect of the BNF algorithm, we compare the positioning performance of applying the BNF algorithm and without applying the BNF algorithm. The background noise of the positioning system includes both thermal noise and ambient light noise. Fig. 14 shows the CDF of the positioning error e_{SGD} of applying BNF algorithm and without applying BNF algorithm. It can be seen that by applying the BNF algorithm, the positioning error e_{SGD} can be significantly reduced, and the average positioning error is reduced from 8.84cm to 1.77cm.

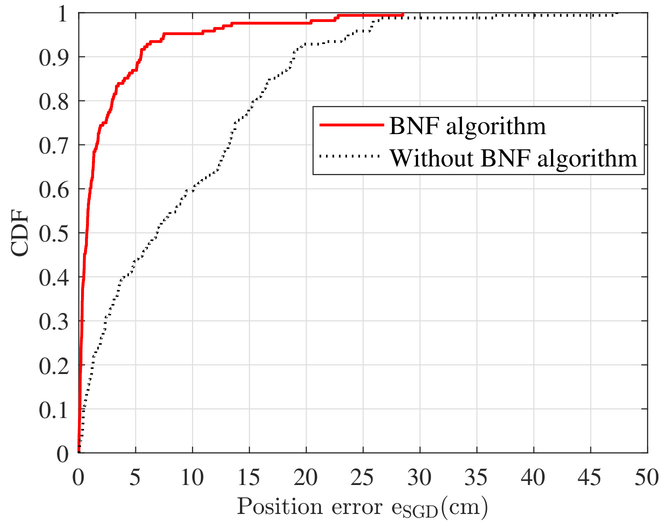

Fig. 14: CDF of the positioning error e_{SGD} of applying BNF algorithm and without applying BNF algorithm.

VII. Conclusions

In this paper, we proposed centimeter-level 3D mobile online VLP schemes for the UE with the multiple PDs and one IMU. We first formulated the positioning problem as an NLS problem by considering arbitrary UE orientation, and obtained the UE location via the SQP positioning schemes. Then, in order to improve the accuracy, we turn to a deep learning method and developed SGD positioning networks. Moreover, we designed a 3D single-lamp-multi-PDs positioning system prototype, where RaspberryPi 4 Model B is used as the positioning signal processor and data memory. Based on the designed VLP system prototype, we examined two positioning schemes for the arbitrary UE orientation scenarios, and the corresponding positioning accuracy can reach 26.36cm and 1.77cm for LS-AO and SGD-AO schemes, respectively. Moreover, for the vertically up UE orientation scenarios, the developed LS-VU and SGD-VU positioning schemes can achieve 16.8cm and 0.7cm positioning accuracy, respectively. Under the same conditions, the positioning error of the proposed positioning schemes is significantly lower than that of the existing methods. In addition, we provided the first publicly available RSS and orientation measured database of 3D VLP systems.

References

[1] Y. Zhuang, Y. Li, L. Qi, H. Lan, J. Yang, and N. El-Sheimy, "A two-filter integration of mems sensors and wifi fingerprinting for indoor positioning," *IEEE Sensors J.*, vol. 16, no. 13, pp. 5125–5126, Jul. 2016.

[2] C. Qi, F. Amato, M. Alhassoun, and G. D. Durgin, "A phase-based ranging method for long-range rfid positioning with quantum tunneling tags," *IEEE J. Radio Freq. Identification*, vol. 5, no. 2, pp. 163–173, Jun. 2021.

[3] R. Kusche, S. O. Schmidt, and H. Hellbrück, "Indoor positioning via artificial magnetic fields," *IEEE Trans. Instrum. Meas.*, vol. 70, pp. 1–9, Apr. 2021.

[4] H. Yao, H. Shu, X. Liang, H. Yan, and H. Sun, "Integrity monitoring for bluetooth low energy beacons rssi based indoor positioning," *IEEE Access*, vol. 8, pp. 215173–215191, Nov. 2020.

[5] X. Shan and Z. Shen, "Miniaturized uhf/uwb tag antenna for indoor positioning systems," *IEEE Antennas Wireless Propag. Lett.*, vol. 18, no. 12, pp. 2453–2457, Dec. 2019.

[6] J. Hao, J. Chen, and R. Wang, "Visible light positioning using a single led luminaire," *IEEE Photon. J.*, vol. 11, no. 5, pp. 1–13, Oct. 2019.

[7] H. Li, H. Huang, Y. Xu, Z. Wei, S. Yuan, P. Lin, H. Wu, W. Lei, J. Fang, and Z. Chen, "A fast and high-accuracy real-time visible light positioning system based on single led lamp with a beacon," *IEEE Photon. J.*, vol. 12, no. 6, pp. 1–12, Dec. 2020.

[8] X. Yu, J. Wang, and H. Lu, "Single led-based indoor positioning system using multiple photodetectors," *IEEE Photon. J.*, vol. 10, no. 6, pp. 1–8, June. 2018.

[9] T. Akiyama, M. Sugimoto, and H. Hashizume, "Time-of-arrival-based smartphone localization using visible light communication," in *2017 International Conference on Indoor Positioning and Indoor Navigation (IPIN)*, pp. 1–7, Nov. 2017.

[10] C. Amini, A. Taherpour, T. Khattab, and S. Gazor, "Theoretical accuracy analysis of indoor visible light communication positioning system based on time-of-arrival," in *2016 IEEE Canadian Conference on Electrical and Computer Engineering (CCECE)*, pp. 1–5, May. 2016.

[11] S.-Y. Jung, S. Hann, and C.-S. Park, "Tdoa-based optical wireless indoor localization using led ceiling lamps," *IEEE Trans. Consum. Electron.*, vol. 57, no. 4, pp. 1592–1597, Nov 2011.

[12] S.-H. Yang, H.-S. Kim, Y.-H. Son, and S.-K. Han, "Three-dimensional visible light indoor localization using aoa and rss with multiple optical receivers," *J. Lightw. Technol.*, Jul. 2014.

[13] S. M. Sheikh, H. M. Asif, K. Raahemifar, and F. Al-Turjman, "Time difference of arrival based indoor positioning system using visible light communication," *IEEE Access.*, vol. 9, pp. 52113–52124, Mar. 2021.

[14] W. Xu, J. Wang, H. Shen, H. Zhang, and X. You, "Indoor positioning for multiphotodiode device using visible-light communications," *IEEE Photon. J.*, vol. 8, no. 1, pp. 1–11, Feb. 2016.

[15] I. M. Abou-Shehada, A. F. AlMuallim, A. K. AlFaqeh, A. H. Muqaibel, K.-H. Park, and M.-S. Alouini, "Accurate indoor visible light positioning using a modified pathloss model with sparse fingerprints," *J. Lightw. Technol.*, vol. 39, no. 20, pp. 6487–6497, Jul. 2021.

[16] J. W. H. L. D. C. J. J. Hongyao Chen Wei Han. and L. Feng, "High accuracy indoor visible light positioning using a long short term memory-fully connected network based algorithm," *Opt. Express*, vol. 28, no. 5, pp. 178–184, Nov 2021.

[17] A. H. A. Bakar, T. Glass, H. Y. Tee, F. Alam, and M. Legg, "Accurate visible light positioning using multiple-photodiode receiver and machine learning," *IEEE Trans. Instrum. Meas.*, vol. 70, pp. 1–12, Dec. 2021.

[18] B. Lin, X. Tang, Z. Ghassemlooy, C. Lin, and Y. Li, "Experimental demonstration of an indoor vlc positioning system based on ofdma," *IEEE Photon. J.*, vol. 9, no. 2, pp. 1–9, Feb. 2017.

[19] T. Sato, S. Shimada, H. Murakami, H. Watanabe, H. Hashizume, and M. Sugimoto, "Alisa: A visible-light positioning system using the ambient light sensor assembly in a smartphone," *IEEE Sensors J.*, vol. 22, no. 6, pp. 4989–5000, Apr. 2022.

[20] N. Huang, C. Gong, J. Luo, and Z. Xu, "Design and demonstration of robust visible light positioning based on received signal strength," *J. Lightw. Technol.*, vol. 38, no. 20, pp. 5695–5707, Jun. 2020.

[21] Z. Wei, Q. Xue, X. Sun, and S. Zhao, "Indoor visible light positioning based on adaptive filtering," in *2021 IEEE International Conference on Information Communication and Software Engineering (ICICSE)*, pp. 294–298, Apr. 2021.

[22] X. Sun, Y. Zhuang, J. Huai, L. Hua, D. Chen, Y. Li, Y. Cao, and R. Chen, "Rss-based visible light positioning using non-linear optimization," *IEEE Internet Things J.*, pp. 1–1, Mar. 2022.

[23] P. Du, S. Zhang, C. Chen, H. Yang, W.-D. Zhong, R. Zhang, A. Alphones, and Y. Yang, "Experimental demonstration of 3d visible light positioning using received signal strength with low-complexity trilateration assisted by deep learning technique," *IEEE Access.*, vol. 7, pp. 93986–93997, Jul. 2019.

[24] C.-W. Hsu, S. Liu, F. Lu, C.-W. Chow, C.-H. Yeh, and G.-K. Chang, "Accurate indoor visible light positioning system utilizing machine learning technique with height tolerance," in *OFC.*, pp. 1–3, Jun. 2018.

[25] D.-C. Lin, Y.-C. Wu, C.-Y. Hong, S.-H. Song, Y.-S. Lin, Y. Liu, C.-H. Yeh, and C.-W. Chow, "3-d indoor visible light positioning (vlp) system based on linear regression or kernel ridge regression algorithms," in *GC Wkshps.*, pp. 1–6, Mar. 2020.

[26] P. Du, S. Zhang, A. Alphones, and C. Chen, "Faster deployment for indoor visible light positioning using xgboost algorithms in industrial internet-of-things," in *IECON 2021 – 47th Annual Conference of the IEEE Industrial Electronics Society*, pp. 1–7, Nov. 2021.

[27] A.-C. Anastou, K. K. Delibasis, A.-A. A. Boulogeorgos, H. G. Sandalidis, A. Vavoulas, and S. K. Tasoulis, "A low complexity indoor visible light positioning method," *IEEE Access*, vol. 9, pp. 57658–57673, Apr. 2021.

[28] A. H. Saboundji, S. Meziane, M. Dahmani, A. Meche, and M. Keche, "Accurate visible light positioning system using neural network," in *2022 7th International Conference on Image and Signal Processing and their Applications (ISPA)*, pp. 1–5, Jun. 2022.

[29] J. B. Kuipers., "Quaternions and rotation sequences: A primer with applications to orbits, aerospace and virtual reality," *USA: Princeton Univ. Press,*, vol. 66, no. 1, 1999.

[30] S. Feng, R. Zhang, W. Xu, and L. Hanzo, "Multiple access design for ultra-dense vlc networks: Orthogonal vs non-orthogonal," *IEEE Trans. Commun.*, vol. 67, no. 3, pp. 2218–2232, Mar. 2019.

[31] R. Zhang, Y. Cui, H. Claussen, H. Haas, and L. Hanzo, "Anticipatory association for indoor visible light communications: Light, follow me!," *Wireless Commun.*, vol. 17, no. 4, pp. 2499–2510, Apr. 2018.

[32] M. D. Soltani, Z. Zeng, I. Tavakkolnia, H. Haas, and M. Safari, "Random receiver orientation effect on channel gain in lifi systems," in *IEEE WCNC.*, pp. 1–6, Apr. 2019.

[33] J. H. Y. L. Z. Wen H. Liu., *Optimization: Modeling, Algorithm and Theory*, Higher Education Press, 2020.

Shuai Ma received the B.S. and Ph.D. degrees in communication and information systems from Xidian University, Xi'an, China, in 2009 and 2016, respectively. From 2014 to 2015, he was a Visiting Scholar with the Department of Electrical and Computer Engineering, Texas A&M University, College Station, TX, USA. From 2016 to 2019, he has been an associate Professor with the School of Information and Control Engineering, at the China University of Mining and Technology, Xuzhou, China. From 2019 to 2022, he worked as a Postdoctoral Fellow with Telecom Paris, France. Since 2023, he has been an Associate Researcher at Peng Cheng Laboratory, Shenzhen, China. His research interests include semantic communications, visible light communications, and network information theory.

Bing Li received the B.E. degree from Henan Polytechnic University, Henan, China in 2020 and the Master degree from China University of Mining and Technology, Xuzhou, China in 2023. His research interests are mainly in visible light communication and visible light positioning.

GuanJie Zhang is currently pursuing the master's degree with China University of Mining and Technology. His research interests currently focus on visible light communication, semantic communication.

Hang Li received the B.E. and M.S. degrees from Beihang University, Beijing, China, in 2008 and 2011, respectively, and the Ph.D. degree from Texas A&M University, College Station, TX, USA, in 2016. He was a postdoctoral research associate with Texas A&M University (Sept. 2016 – Aug. 2017) and University of California-Davis (Sept. 2017 – Mar. 2018). After being a visiting research scholar (Apr. 2018 – June 2019) at Shenzhen Research Institute of Big Data, Shenzhen, China, he has been a research scientist since June 2019. His current research interests include wireless networks, Internet of things, stochastic optimization, and applications of machine learning.

Chen Qiu received the Ph.D. degree from Beijing University of Posts and Telecommunications, Beijing, China, in 2020 and the B.E. degree from Beijing University of Posts and Telecommunications, Beijing, China and Queen Mary University of London, London, England in 2013. He was a visiting scholar in the Department of Electrical and Computer Engineering, University of California at Davis (2016-2017) and Department of Electrical and Computer Engineering, Texas A&M University (2015-2016). He is currently a postdoctoral researcher in Peng Cheng Laboratory, Shenzhen, China. His research interests include UAV-assisted wireless network, integrated sensing and communication and machine learning in wireless systems.

Chuang Yu received the Ph.D. from Institut Polytechnique de Paris, Paris, France, in 2021 and the Master degree from Beihang University, Beijing, China in 2017 and the B.E. degree from Civil Aviation University of China, Tianjin, China in 2014. He was a Research Associate (2021-2023) in the Cognitive Robotics Lab, Department of Computer Science, University of Manchester, Manchester, UK. Currently, He is a Research Fellow at UCL Interaction Centre, University College London, London, UK. His interests are cognitive-social robotics, Human-Robot Interaction, affective AI, and generative AI.

Shiyin Li received the Ph.D. degree in information and communication engineering from the China University of Mining and Technology, Xuzhou, China, in 2010. Since 2010, he has been a Professor with the School of Information and Control Engineering, China University of Mining and Technology, where he is the Head of the Department of Information Engineering. His research interests include wireless communication and network congestion control.

Chao Shen (Member, IEEE) received the B.S. degree in communication engineering and the Ph.D. degree in signal and information processing from Beijing Jiaotong University (BJTU), Beijing, China, in 2003 and 2012, respectively. He was a Visiting Scholar with the University of Maryland, College Park, MD, USA. From 2013 to 2022, he is an Associate Professor with the State Key Laboratory of Rail Traffific Control and Safety, BJTU. He is currently a Senior Research Scientist with the Shenzhen Research Institute of Big Data, Shenzen, China. His research interests include in large-scale networks optimization and signal processing for wireless communications.